Influence of concrete's mechanical properties on the cracking of concrete dams

Adrian Ulfberg

Department of Civil, Environmental and Natural Resources Engineering, Luleå University of Technology, Luleå, Sweden.
E-mail: adrian.ulfberg@ltu.se

Andreas Seger

SINTEF Narvik, Narvik, Norway
UiT - The Arctic University of Norway, Tromsø, Norway
E-mail: andreas.seger@uit.no

Dipen Bista

SINTEF Narvik, Narvik, Norway
Norwegian University of science and technology, Trondheim, Norway
E-mail: dipen@tek.norut.no

Marie Westberg Wilde

Soil- and rock mechanics, KTH Royal Institute of Technology, Stockholm, Sweden
E-mail: marie.westberg.wilde@afconsult.com

Fredrik Johansson

Soil- and rock mechanics, KTH Royal Institute of Technology, Stockholm, Sweden
E-mail: fredrik.johansson@byv.kth.se

Oisik Das

Department of Civil, Environmental and Natural Resources Engineering, Luleå University of Technology, Luleå, Sweden.
E-mail: Oisik.das@ltu.se

Gabriel Sas

Department of Civil, Environmental and Natural Resources Engineering, Luleå University of Technology, Luleå, Sweden.
E-mail: gabriel.sas@ltu.se

Analytical methods of structural stability assessment of concrete dams are often too simple and thus conservative in their predictions. Without the actual foundation geometry, capacity for some rigid body failure modes are underestimated. This is problematic when deciding upon remediation activities of a dam that is considered unstable and may divert the restoration activities from where they are most impactful. In a previous study by Sas et al. 2019 where a section of an existing dam was scaled down and tested experimentally, the model indicated that several areas were experiencing large stresses, potentially leading to failure. This raised the research question whether another type of failure would occur for different material properties. Therefore, this paper delves into a probabilistic numerical approach, through finite element analysis, to evaluate dam stability based on randomization of a number of material properties such as modulus of elasticity, tensile strength, compressive strength, and fracture energy. The variation of the aforementioned material properties did not impact the failure mode, which was consistent among a broad range of material strengths.

Keywords: Concrete dams, Model test, Numerical analysis, Material randomization

1. Introduction

At present, many existing and functioning concrete dams are nearing the end of their service life. In Sweden and Norway, it is estimated that ca.14000 concrete dams (Sas et al. 2019) exist where many of them will need retrofitting or to be replaced in the near future. Concrete dams are usually assessed by analytical methods, such as the shear friction method or the limit equilibrium method, using deterministic input variables. These methods are usually simplified to the extent where they become overly conservative when dealing with assessment of an existing dam structure. Moreover, with the adoption of stricter safety coefficients many dams are assessed as unstable.

The current paper builds upon previous work reported by Sas et al. (2019) on a specific section of Kalhovd dam, a concrete buttress dam in Norway, which was deemed unstable during assessment. This section of the dam is

Proceedings of the 31st European Safety and Reliability Conference
Edited by Bruno Castanier, Marko Cepin, David Bigaud, and Christophe Berenguer
Published by Research Publishing, Singapore.
ISBN: 978-981-18-2016-8; doi:10.3850/978-981-18-2016-8_549-cd

distinguished by two large asperities in the interface between the dam pillar and foundation, similar to shear keys. These 1st order asperities are believed to have a positive effect on the stability in at least one of the commonly evaluated failure modes. However, their influence on the stability is difficult to model with analytical calculation methods. Sas et al. (2019) investigated the influence of these 1st order asperities on the stability of concrete buttress dams experimentally and numerically. Four tests were performed on specimens (models), replicating an existing pillar (the prototype) in a real dam, scaled down 1:5. Non-linear 2D finite element models were implemented as a complement to these scale model tests.

During testing of one of the scale models to failure under a certain loading scheme, where only the simulated hydrostatic pressure was scaled up, signs of overstressing in several points was observed. Most of these highly stressed zones were located around the doorway and large signs of stress concentrations could be seen beneath it next to the back asperity (see Figure 1). However, very few of these highly stressed areas was the reason for the failure of the model as rupture of the concrete suddenly occurred diagonally from one of the macro asperities.

Although, the study by Sas et al. (2019) was valuable in revealing the effect of macro asperities in a concrete buttress dam on the structural integrity, it is unclear if the overstressed areas could have led to a different kind of failure for a dam body with different material properties. The current study attempts to identify how Sas et al. (2019) might be influenced by considering varying material parameters by means of probabilistic non-linear finite element modelling.

2. Scale model tests

For the sake of brevity, the scale model test performed by Sas et al. (2019) is described briefly in this paper and the reader is referred to the full aforementioned report for further details. The aim of the study by Sas et al. (2019) was to investigate the influence of the 1st order asperities, in the rock-concrete interface, on the stability against sliding and overturning. Test were performed on four different scale models of pillar 49 of Kalhovd dam in Norway. This particular pillar was selected for the study as it did not meet the safety requirements imposed by governmental requirements (NVE, 2005) during its assessment. These assessments included analytical methods which did not account for its macro asperities. The four scale models differed geometrically by including the front- or back asperity, both asperities, and one reference sample model without any asperities. This paper focuses only on the scale model that included both asperities.

The pillar was scaled down 1:5, using dimensional analysis (Buckingham, 2019). Similarity criteria were applied to the loads, geometry, and material properties. Derivations of the criteria and properties are described in Sas et al. (2019). The pillar was unreinforced and match cast with the foundation where any cohesion between the foundation and pillar was prevented by applying rubber paint on the interface on the foundation side. This rubber paint was ground of after hardening of the pillar. Cube samples from each cast were subjected to tilt angle tests, before and after the paint was ground of.

To obtain the desired strength of model pillar material, the model concrete was developed with 1 part cement, 0.6-part water and 3-part sand of 0/4 mm. Material parameters, given for the model concrete samples, which are considered relevant for this numerical study is given in Table 1.

The test setup consisted of a loading system and a guiding system. The loading system involving hydraulic jacks, a pulley with weights, and a loading beam was designed to replicate the scaled hydrostatic pressure, uplift pressure and ice pressure. Two of the hydraulic jacks were connected to a beam adjacent to the pillar whose purpose was to distribute the forces from the hydraulic jacks to more realistically simulate hydrostatic pressure. The guiding system was needed, due to the lack of front plate, to prevent the pillar from displacing out from its original plane. A schematic view of the test set up is shown in is shown in figure 1 below.

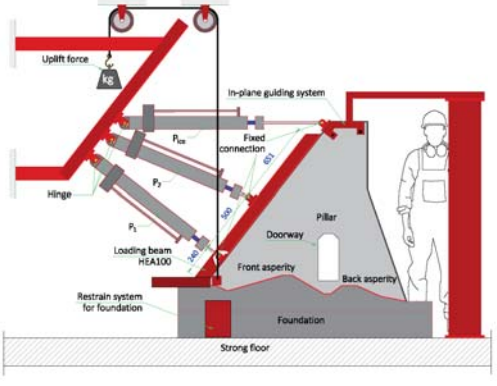

Fig. 1. Test setup for the scale mode tests performed in Sas et al. 2019

The loading scheme of the test studied in this article consisted of only simulating the hydrostatic pressure from water using the P1 and P2 actuators (see Figure 1). For this scheme, the model failed at an applied load of 37 kN. The other case study, where ice and uplift pressure was also simulated, the resistance of the same interface was tested against overturning. The latter case will not be discussed here, for further details see Sas et al. (2019).

The samples were monitored using optical, photogrammetric 3D measurements. Digital Image Correlation (DIC) and point-tracking methods were used to monitor the tested specimens in real-time. Linear variable differential transformers (LVDT's) were also implemented to monitor the displacement of the scale models. Figure 2 shows the position of the LVDT's and their arrows denote the direction of measurements for the individual LVDT.

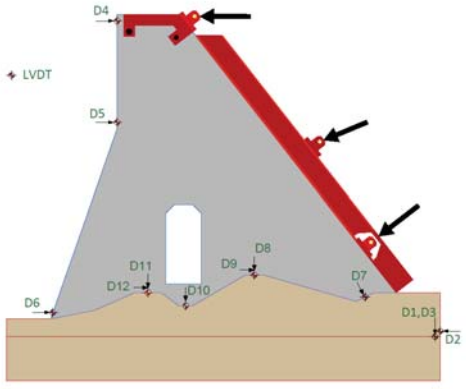

Fig. 2. Location and numbering of LVDT's (named D1-D12) and positions and directions of hydraulic presses. Sas et al. 2019

3. Nonlinear finite element modelling

3.1. *Model*

The software used for the analysis was ATENA Engineering 2D v5. The numerical model was previously used in Sas et al. (2019) and is shown with its finite element mesh in figure 3. The two applied loads are shown with large arrows.

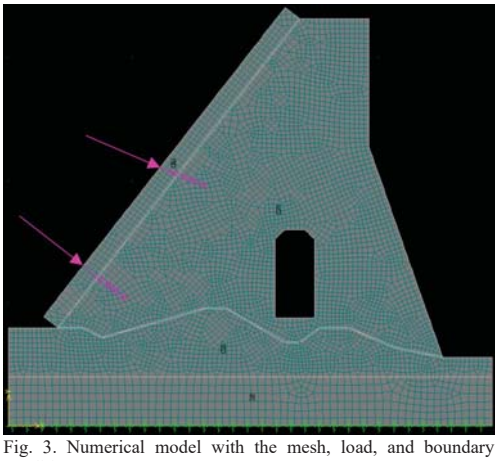

Fig. 3. Numerical model with the mesh, load, and boundary conditions

The finite element mesh used in the analysis model was determined after performing a mesh sensitivity analysis in which the consistency of the results was weighed against the computational time (Sas et al. 2019). Eight node quadrilateral elements were used in the mesh. The concrete in the pillar was simulated by a fracture plastic model where the input material parameters in the deterministic model, later serving as mean values in the randomization, are given in Table 1. Modulus of elasticity, tensile strength, compressive strength, and plastic strain at peak stress are given from the results from the tests of the model concrete samples in Sas et al. (2019).

Table 1. Material values for the deterministic model

Modulus of elasticity, E [MPa]	8875
Poisson's ratio, ν [-]	0.2
Tensile strength, f_t [MPa]	0.72
Compressive strength, f_c [MPa]	9.9
Fracture energy, G_f [N/m]	3.748
Plastic strain at strength f_c, ε_{CP} [-]	1.63×10^{-3}
Critical compressive displacement*, w_d [m]	-5×10^{-4}
Reduction of compressive strength due to cracks*, r_c^{lim} [-]	0.8
Crack shear stiffening factor*, S_F [-]	20
Specific material weight, ρ [MN/m^3]	1.516×10^{-2}

*Software default value

Fracture energy was never tested during the study (Sas et al. 2019). The model concrete used in the scale model test had a maximum aggregate size of 4 mm. Conforming to findings by Schneemeyer et al. (2014), and Tongyan et al. (2011), the fracture energy of the model concrete used in the casting the pillar, was assumed to be low and not representable by formulae as expressed by e.g. fib (2010).

The model that was decided upon to express the fracture energy in the analysis was derived by Tongyan et al (2011) where the fracture energy, G_F, is approximated by the maximum aggregate size, d_{max}:

$$G_F = 0.36 \times {d_{max}}^{1.69}\ [N/m] \quad (1)$$

The interface was modelled using a material model based on the Mohr-Coulomb criterion with tension cut off (Červenka et al. 2020). Due to the interface in the scale model test being processed to break bonding, the tensile strength and cohesion of the interface was set to zero and proved to still be numerically stable. The friction angle was based on the average value given from tilting table tests on cylindrical specimens from the same cast.

The stiffnesses of the interface and the friction coefficient are given in able 2. The minimal stiffness is the stiffness of the interface in its open state (i.e. no contact) and only serves for numerical stability. In accordance with Červenka

et al. (2020), the minimum stiffness was set to one thousandth of the closed state.

Table 2. Interface stiffnesses and its friction coefficient

Normal stiffness, K_{nn} [MN/m^3]	4.438×10^6
Tangential stiffness, K_{tt} [MN/m^3]	2.773×10^6
Friction coefficient [-]	0.716
Minimal normal stiffness, K_{nn}^{MIN} [MN/m^3]	4.438×10^3
Minimal tangential stiffness, K_{tt}^{MIN} [MN/m^3]	2.773×10^3

Linear springs were used for the boundary conditions as the foundation for the pillar in question was placed on top of a gypsum layer in which crushing was seen after the test. This induced some deformation and rotation of the test setup. The stiffness of these springs was determined by using deformation given by the DIC from fixed points of the foundation. (Sas et al. 2019)

In the model tests, loading was applied by hydraulic jacks attached to a HEA 100 beam which distributed the force to an equivalent hydrostatic pressure increasing linearly from top to bottom. The numerical model used plane stress elements with a linear elastic material model and an equivalent bending stiffness as the HEA 100 beam.

An interface was implemented in between the elements representing the beam and the pillar. The stiffness of this interface was based on numerical tests and was consequently set to 638 MN/m^3 for the normal stiffness and 400 MN/m^3 for its tangential stiffness. The cohesion was set to 1 MPa, tensile strength to 0.1 MPa, and the friction coefficient was given a value of 0.85.

The foundation elements also implemented a fracture plastic constitutive model with material parameters equivalent to that of C30/37 concrete. Reinforcement in the foundation for the numerical model was neglected.

The loading scheme used in the numerical analysis consisted of initially applying the automatically generated self-weight of the of the modelled elements. Then, two point loads, simulating the hydraulic jacks in the tests, were applied. The bottom point load consisted of 60% of the total applied load and upper point load of the remaining 40%.

Simulations were load controlled with the arc length method as the solver type.

3.2. *Parameter randomization*

The variables considered to be the most impactful in the study and chosen for the randomization process were the compressive strength, tensile strength, fracture energy, and modulus of elasticity. Instead of adopting a random field approach where the parameter varies spatially within the FE-mesh of the macro element, the whole macro element was given a fixed value for the randomized parameters. The parameter randomization process was performed in the probabilistic module, FREET; a module to ATENA Engineering 2D. Sampling was performed with Latin Hypercube Sampling (LHS). The mean values for the analysis were based of the deterministic values obtained through laboratory testing. Table 3 show the maximum and minimum values given from the randomization, the coefficients of variance (CoV) used, and the mean input values.

Table 3. Mean, maximum, and minimum values of material parameters randomized

	Modulus of elasticity, E [MPa]	Tensile strength, f_t [MPa]	Compressive strength, f_c [MPa]	Fracture energy, Gf [N/m]
Mean	8875	0,72	9,90	3,75
Max	11350	0,99	12,66	5,32
Min	6878	0,37	7,67	1,75
CoV	0,15	0,18	0,1	0,2

For the compressive strength of the concrete, a lognormal distribution was assumed as recommended by Silvestri, et al. (2008) and Johansson & Westberg Wilde (2016). Similarly, the modulus of elasticity was assumed to have the same distribution function as the parameters in question are thought to be highly correlated (Noguchi & Nemati, 2007). A Weibull distribution function was considered for the randomized tensile parameters. The CoV's were based of Strauss et al. (2009).

The correlation matrix used for the material parameters is based on Havlasek & Pukl (2017). In the upper triangle of Table 4, the expected values of correlation are shown and the given values, using a simulated annealing optimization technique, are shown in the lower triangle.

Table 4. Expected values of correlation in the upper triangle and given correlation

	E	f_t	f_c	G_f
E	1	0.6	0.9	0.5
f_t	0.599	1	0.6	0.9
f_c	0.899	0.601	1	0.6
G_f	0.499	0.899	0.599	1

The sample size for the randomized numerical models was iteratively chosen by means of increasing the size until parameter sensitivities started to converge. At a sample size of 64, the sensitivities were only slightly different from the previous sample size of 32 and was considered to provide satisfactory accuracy. A study by Vořechovský (2010) showed that the LHS sampling technique could provide quick convergence for number of different functions with a relatively low amount of simulations.

4. Results

The load-displacement curves for every numerical analysis is shown in figure 4 below. Black curves are from the numerical simulations and the red curve is from the model tests.

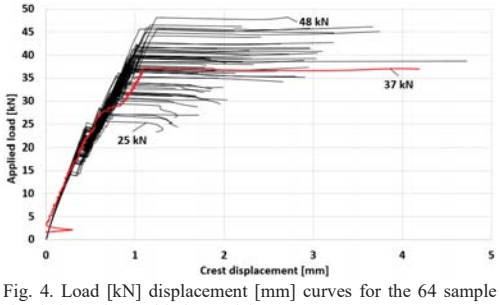

Fig. 4. Load [kN] displacement [mm] curves for the 64 sample simulations along with the model tests

The maximum applied load in one of the analyses was 48 kN. Outliers were found within the sample set and were deemed to be caused by numerical errors attributed to the interface elements. Disregarding these outliers, the minimum load that a sample was subjected to before experiencing a clear failure was 25 kN.

Following Figures 5, 6, 7, and 8 show scatterplots of the material parameter versus the total applied load. Scatterplots are shown in sequence of modulus of elasticity, tensile strength, compressive strength, and fracture energy. The models with numerical instability whose results were considered as outliers are shown in red and are omitted in the calculated r-squared values.

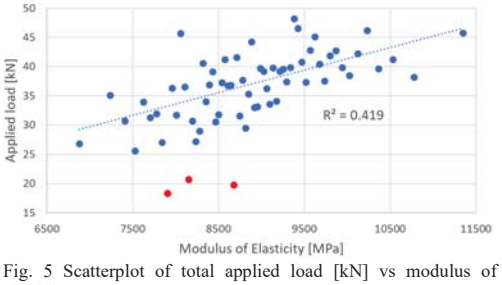

Fig. 5 Scatterplot of total applied load [kN] vs modulus of elasticity [MPa]

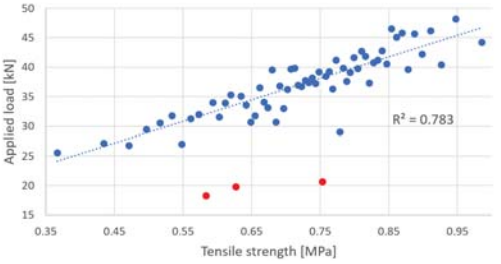

Fig. 6. Scatterplot of total applied load [kN] vs tensile strength [MPa]

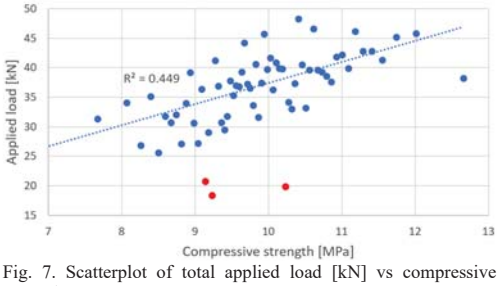

Fig. 7. Scatterplot of total applied load [kN] vs compressive strength [MPa]

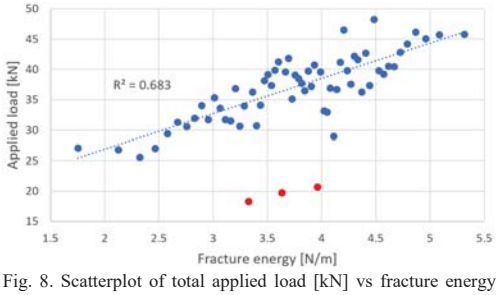

Fig. 8. Scatterplot of total applied load [kN] vs fracture energy [N/m]

Table 5 show the sensitivities for the applied load from the individual randomized parameters as given by ATENA's randomization module FREET. These sensitivities use spearman rank correlation (Novák et al. 2002) and they show large dependency on the tensile parameters.

Table 5. Sensitivities given for the numerical analysis of the 64 samples

	E	f_t	f_c	G_f
Sensitivity	0.678	0.856	0.690	0.748

5. Analysis and discussion

Post-processing of the sample set showed a regularly emerging cracking pattern. Cracking first started in the bottom of the doorway connecting to the back asperity. Further in the analysis, cracks emerged in the middle of the doorway and next to the bottom corner on the opposite side of the first crack. At the near end of the analysis, when the load displacement curves went horizontal, sudden cracking occurred from the front of the dam model towards the front asperity and diagonally from the top of the doorway. Figure 9 shows the cracked elements at the last load step for simulation 3. This simulation was arbitrarily chosen among the models and is indicative of the common crack pattern. Note that the figure only shows the cracked elements and is not indicative of crack widths.

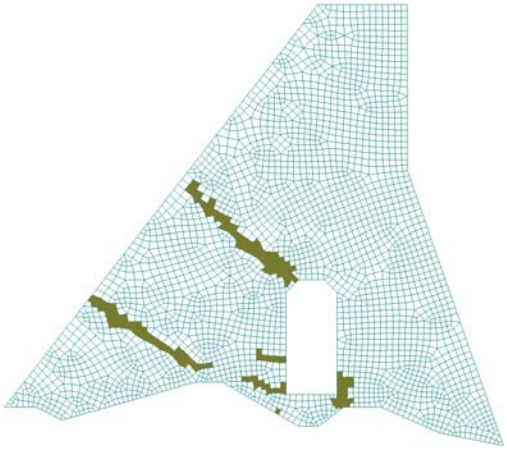

Fig. 9. Cracked elements at the last load step for simulation 3

Crack patterns at the last steps of the analysis varied between the models but was not assumed to be the cause of failure as most of them emerged after the regularly occurring crack pattern shown in figure 9.

The strain measurements from the model test performed by Sas. et al. 2019 as measured by DIC is shown in figure 10 below.

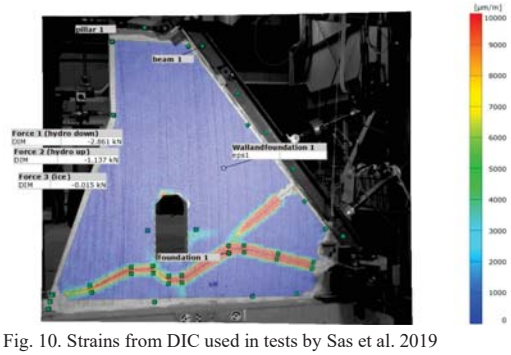

Fig. 10. Strains from DIC used in tests by Sas et al. 2019

It can be seen from the previous figures that the crack pattern between the numerical simulation and the scale model test is similar. The crack width of the diagonal crack in the top of the doorway for the finite element simulation is very small and was not captured by DIC in the scaled model tests due to low sampling rate. However, this crack could be seen upon close inspection.

Leading up to failure, the numerical analyses revealed that the interface was in contact only in the parts around the back asperity. This was caused by the crack in the bottom of the doorway as this allowed the specimen to rotate around the upstream edge next of the back asperity (beneath the doorway). The bottom front part of the buttress model then acted similarly to a corbel for the load exercised by the hydraulic jack where the large diagonal crack from the front asperity emerged. The way the numerical models failed is shown schematically in figure 11. Stress trajectory plot is based on the trend of the stress tensors shown before failure of the samples.

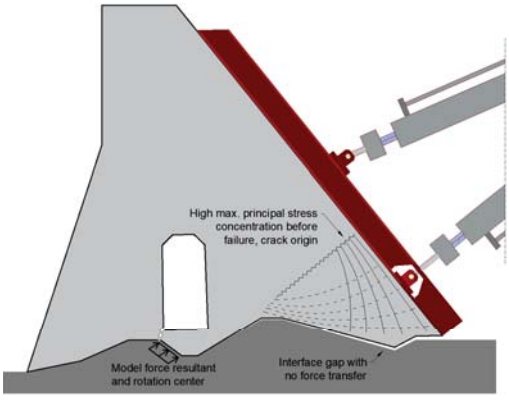

Fig. 11. Failure mechanism in the numerical models

Questions may arise whether the steel beam was able to distribute the pressure from the hydraulic presses adequately. Looking at the numerical simulations, the interface between the loading beam and the pillar had a stress distribution similar to the linear stress distribution the pillar would experience from hydrostatic water pressure. The reference sample without asperities in the study by Sas et al. (2019) included a pressure film between the loading beam and the pillar where the stresses recorded also implied that the beam sufficiently distributed the load.

The sensitivities and the r-squared values given resulted from the analysis show a large correlation between the tensile parameters and the ultimate load. Since no reinforcement was present in neither the model and numerical models, the failure is brittle, and forces will not be able to bridge the crack when all of the fracture energy has been expended. The results given from the sensitivity analysis are thus reasonable with the way the tensile stresses

develop in the buttress section under the loading pattern. It is however undisclosed whether this failure would be governing had the front plate been accounted for in the analysis. This is a subject of further studies.

Due to these stress developments, the strength could be significantly higher while still exhibiting the same type of failure pattern. The overstressed areas that could be seen during the scaled model test was never the cause of failure even with large differences between the maximum and minimum values for the material parameters.

Noteworthy is that the test specimen failed at loads more than 3 times above the equivalent design load for the hydrostatic pressure of the dam. Even the worst performing numeric model surpassed the design hydrostatic load by a factor of more than 2. This shows that the macro asperities contribute heavily to the sliding capacity of the dam section as past analytical assessment of this section deemed it to be unstable in both the sliding and the overturning failure mode Sas et al. (2019).

In the existing dam section, a comparable crack pattern has been observed from the front asperity (Sas et al. 2019). The model test and the study provided might indicate a possible origin of this crack. Although, many factors could be the cause of the crack. In these simulations, the equivalent hydrostatic pressure was the only simulated load and thus caused the failure. The hydrostatic pressure has a force resultant that occurs at a relatively low height on the dam body in contrast to the commonly assumed position of the ice load, near the dam crest. It can be theorized that while the capacity of the real dam may not be governed by this type failure due the inclusion of e.g. reinforcement, the same behavior where the specimen overturn and lose contact with the interface might occur due to the ice load. Therefore, the same diagonal crack opening could be achieved by the seasonal ice load at a lower total applied force than the equivalent load given in this study.

6. Conclusions

This paper studied ultimate limit state behavior of a section of a concrete buttress dam, that was scaled down and tested using finite element analysis with parameter randomization. The influence of the model concrete's material parameters namely, modulus of elasticity, tensile strength, compressive strength, and fracture energy was studied based upon the experimental tests performed by Sas et al. 2019. The section consisted of a doorway with two macro asperities along the foundation interface. The cause of failure was consistently caused by principal stress concentrations where the crack initiated at the front of the pillar and progressed towards the front asperity. No other types of failure were exhibited when varying the aforementioned material parameters. This affirms that large macro asperities can have a significant impact on the sliding stability. Thus, macro asperities could lead to non-rigid body failures being governing for the ultimate load capacity. This is due to the asperities' positive effect on the sliding stability.

Acknowledgement

The authors are grateful for the funding from the "The Stable Dams" project with the grant number 244029. The authors also express their gratitude to the research program council of Norway, ENERGIX.

References

Buckingham, Edgar. "On Physically Similar Systems; Illustrations of the Use of Dimensional Equations." Physical review 4, no. 4 (1914): 345.

Červenka, V. Jendele, L. Červenka, J. Atena Program Documentation, Part 1, Theory. 2020.

Fédération internationale du béton. "Fib Model Code for Concrete Structures 2010." Berlin, Germany: Ernst & Sohn, 2010.

Havlásek, P. Pukl, R. "Sara Program Documentation." Cervenka Consulting 2017.

Noguchi, T. Nemati, K, M. "Relationship between Compressive Strength and Modulus of Elasticity of High-Strength Concrete." Journal of Structural and Constriction Engineering 60 (August 30 1995).

Novák, D. Teplý, B. Keršner, Z. Vořechovský, M. "Freet Program Documentation." 2002.

NVE. "Retningslinjer for Betongdammer." 2005.

Sas, G. Seger, A. Bista, D. Popescu, C. Arntsen, B. "Stable Dams: Capacity and Resistance." 2020.

Sas, G. Seger, A. Bista, D. Popescu, C. Arntsen, B. Johansson, F. Lia, L. "Influence of Large-Scale Asperities on the Shear Strength of Concrete Dams' Interfaces." 2019.

Schneemayer, A. Schranz, C. Kolbitsch, A. Tschegg, E, K. "Fracture-Mechanical Properties of Mortar-to-Brick Interfaces." Journal of Materials in Civil Engineering 26, no. 9 (October 14 2014).

Silvestri, S. Gasparini, G. Trombetti, T. Ceccoli, C. "Statistical Analysis Towards the Identification of the Accurate Probability Distribution Models for the Compressive Strength of Concrete " In World Conference on Earthquake Engineering. Beijing, China, 2008.

Strauss, A., S. Hoffmann, R. Wendner, and K. Bergmeister. "Structural Assessment and Reliability Analysis for Existing Engineering Structures, Applications for Real Structures." Structure and Infrastructure Engineering 5, no. 4 (August 1 2009): 277-86.

Tongyan, P. Linbings, W. Tutumluer, E. "Experimental Investigation of Aggregate-Mortar Interface Affecting the Early

Fracture Toughness of Portland Cement Concrete.". International Journal of Pavement Research and Technology 4 (2011).

Vořechovský, Miroslav. "Extension of Sample Size in Latin Hypercube Sampling with Correlated Variables." EDITORS, Michael Beer. REC (2010): 3-5.

Wilde Westberg, M. Johansson, F. "Probabilistic Model Code for Concrete Dams." Energiforsk.se, 2016.